The Rb 780-Nanometer Faraday Anomalous Dispersion Optical Filter: Theory and Experiment

B. Yin, L. S. Alvarez, and T. M. Shay
New Mexico State University, Las Cruces, New Mexico

The Faraday anomalous dispersion optical filter may provide ultra-high background noise rejection for free-space laser communications systems. The theoretical model for the filter is reported. The experimental measurements and their comparison with theoretical results are discussed. The results show that the filter can provide a 56-dB solar background noise rejection with about a 2-GHz transmission bandwidth and no image degradation. To further increase the background noise rejection, a composite Zeeman and Faraday anomalous dispersion optical filter is designed and experimentally demonstrated.

I. Introduction

An important technical issue in free-space laser communications and remote sensing is to effectively reject the optical background while efficiently transmitting the signal through the device. In general, an optical filter with high transmission, narrow bandwidth, wide field of view (FOV), and fast temporal response is needed to extract weak, narrow-bandwidth signals from strong, broadband background radiation, such as the ambient daytime solar illumination (Fig. 1).

We have been exploring a new technology, the Faraday anomalous dispersion optical filter (FADOF) [1–9], that provides a solution to this problem. The performance of the FADOF and other existing state-of-the-art narrow-bandwidth optical filters is summarized in Table 1. The noise rejection factor (NRF) is defined as

$$NRF = 10\log\left[\frac{T(\lambda_s)\int_0^\infty \frac{dP_{noise}}{d\lambda}d\lambda}{\int_0^\infty T(\lambda)\frac{dP_{noise}}{d\lambda}d\lambda}\right] \quad (1)$$

where $T(\lambda)$ represents the filter transmission spectrum, $dP_{noise}/d\lambda$ is the incident noise power spectrum, and λ_s is the signal wavelength. High NRF values of the filter mean high rejection for out-of-passband noise and high transmission in the passband. The wide FOV and image-preserving characteristics make the filter useful for optical tracking in addition to optical communications. The interference filter

represents conventional technology and is inexpensive, but it has a broad bandpass at wide FOV. The Lyot [10] filter has a moderate bandpass and moderate FOV, but does not meet the background rejection requirements for free-space laser communications. The atomic resonance optical filter provides a narrow bandpass, wide FOV, and high background noise rejection [11–15]. However, these filters are not image preserving. Therefore, they have limited usefulness in optical tracking. The FADOF clearly shows significant advantages when compared with the other narrow-bandwidth optical filters. In addition to the above advantages, the FADOF is insensitive to mechanical vibrations and misalignment.

This article presents the theoretical and experimental results of studies on the rubidium (Rb) 780-nm FADOF. There is excellent agreement between the theoretical calculation and experimental measurements. The measurements of solar background noise rejection and image quality for the filter are also reported. Finally, a composite filter that has a FADOF and a Zeeman absorption cell is discussed. The background noise rejection of the composite filter is expected to be a factor of 3.5 better than that of the FADOF.

II. Theory

The theoretical framework for resonant Faraday effects has been published by many authors [16–19], so the basic equations are well understood and quite straightforward. However, those articles either lack the treatment for atomic hyperfine structure in the intermediate magnetic-field strength region or are not applied to optical filters. Therefore, a more general formalism using a quantum mechanics treatment of the resonant Faraday effects has been developed [2].

A FADOF consists of an atomic vapor cell placed in a dc magnetic field parallel to the optical path. The cell is situated between 90-deg crossed polarizers (Fig. 2). When linearly polarized light travels along the direction of the magnetic field through the dispersive atomic vapor, a polarization rotation occurs (resonant Faraday effect). Thus, only the narrow frequency band that has a 90-deg polarization rotation will be transmitted with high efficiency.

We assume that (1) optical pumping effects are negligible, because the transmission bands of the FADOF are outside the absorption line centers (for example, the calculated saturation intensity in the filter transmission band of the Rb 780-nm FADOF is about 2 kW/cm^2—4 orders of magnitude higher than the total solar intensity at the Earth's surface) and (2) the magnetic field is homogeneous within the Faraday cell (for inhomogeneous analyses, an integration over the magnetic field along the Faraday cell may be implemented). The FADOF calculation takes into account both Zeeman spectra [20–22] and magneto-optical rotation (Faraday effects). For an atom with a total orbital angular momentum J, nuclear spin I, total angular momentum $F = J + I$, and the projection of the total angular momentum along the direction of the external magnetic field M, the Hamiltonian matrix elements (F, F') for each value of M are

$$\langle IJFM|H|IJF'M\rangle = \Delta E_F \delta(F,F') + \left[\mu B_Z (-1)^{M+J+1+I}(g_J - g_I) \times \sqrt{J(J+1)(2J+1)(2F+1)(2F'+1)} \times \begin{Bmatrix} J & 1 & J \\ F' & I & F \end{Bmatrix} \begin{pmatrix} F & 1 & F' \\ -M & 0 & M \end{pmatrix}\right] \quad (2)$$

where the first term represents the hyperfine interaction energy, the second term represents the external magnetic energy, and [11]

$$\Delta E_F = \frac{h}{2}AK + hB \times \left[\frac{\frac{3}{2}K(K+1) - 2I(I+1)J(J+1)}{2I(2I-1)2J(2J-1)}\right] \quad (3)$$

where $K = F(F+1) - J(J+1) - I(I+1)$, A and B are the magnetic dipole and electric quadruple constants, respectively, for the energy level of interest, μ is the Bohr magneton, B_z is the external magnetic field, and g_J and g_I are the gyromagnetic factors for the total orbital angular momentum and nuclear spin momentum, respectively. The matrix element dependence on M is contained within the 3-J symbol (enclosed by the parentheses), and the matrix element dependence on F is related to a 6-J symbol (enclosed by the curly bracket). These symbols are matrix representations of the spherical coordinate components of the electron wave function for the single atom.

The Zeeman energy levels are readily obtained from the eigenvalues of the Hamiltonian matrix. Figure 3 shows the simplified energy level diagram for the four rubidium transitions in the near infrared and blue. The fine structure energy levels are shown on the left side of the figure. The hyperfine structure energy levels are shown in the middle of the figure and were obtained by adding nuclear spin interaction energy to the fine structure. The magnetic energy levels are shown at the right side of the figure, and show the modification to the hyperfine energy level splittings caused by the addition of the external magnetic field.

Not only do the energy levels split when the magnetic field is applied, but the transition strengths for the different components also change. The Zeeman intensity of each spectral line is proportional to the transition strength denoted by $S_{\pm}(FM, F'M')$, where the subscripts + and − denote the right-circular and left-circular components of the atomic dipole moment vector $\vec{d}$, respectively.

$$S_{\pm}^{1/2}(FM, F'M') = \sum_{\beta}\sum_{\beta'} Y_{\beta FM}^{\gamma} \times \langle \beta FM | d_{\pm} | \beta' F'M' \rangle Y_{\beta' F'M'}^{\gamma'} \quad (4)$$

$$\langle \beta FM | d_{\pm} | \beta' F'M' \rangle = (-1)^{F-M} \times \begin{pmatrix} F & 1 & F' \\ -M & \pm 1 & M' \end{pmatrix} \times \langle \beta F \parallel d \parallel \beta' F' \rangle \quad (5)$$

and

$$\langle \beta F \parallel d \parallel \beta' F' \rangle = (-1)^{J+I+F+1} \sqrt{(2F+1)(2F'+1)} \times \begin{Bmatrix} J & I & F \\ F' & 1 & J' \end{Bmatrix} \langle J \parallel d \parallel J' \rangle \quad (6)$$

where the prime denotes excited states, γ represents perturbed states, β represents diagonalized energy states, Y represents the eigenvector matrix for the Hamiltonian matrix H, and

$$|\gamma FM\rangle = \sum_{\beta} Y_{\beta FM}^{\gamma} |\beta FM\rangle \quad (7)$$

The reduced matrix element $\langle J \parallel d \parallel J' \rangle$ is common to all the hyperfine components of the spectral line and is given by the relation

$$\langle J \parallel d \parallel J' \rangle^2 = \frac{3}{64\pi^4}(2J'+1)h\lambda^3 A_{JJ'} \quad (8)$$

where λ and $A_{JJ'}$ are the wavelength and transition probability between levels J' and J, respectively.

The Rb 780-nm transition is between the ground state $5^2S_{1/2}$ and $5^2P_{3/2}$. Natural Rb has two isotopes with an abundance of 72-percent ^{85}Rb and 28-percent ^{87}Rb. The magnetic energy levels of ^{85}Rb $5^2P_{3/2}$ are shown in Fig. 4, and the spectrum of the relative transition intensities is shown in Fig. 5.

The horizontal axis of Fig. 5 represents the transition frequencies, where 0 is the frequency (approximately 3.85 THz) corresponding to 780 nm. The two inside and two outside hyperfine transition groups are from the ^{85}Rb and ^{87}Rb isotopes, respectively. The relative intensity and transition frequency of each hyperfine component depend on the magnetic field.

The observed Zeeman spectrum depends on the viewing direction and the polarization. In our calculations, we assume that the incident radiation is linearly polarized transverse to the magnetic field; therefore, the polarization can be resolved into equal-amplitude left- and right-circularly polarized components.

The Faraday rotation is a direct result of the difference in the frequency dependence of the phase delay between the right- and left-circularly polarized light. The Faraday rotation angle $\phi(\omega)$ is given by

$$\phi(\omega) = \frac{\omega L}{2c} Re[\tilde{n}_+(\omega) - \tilde{n}_-(\omega)] = \frac{\omega L}{2c}[n_+(\omega) - n_-(\omega)] \quad (9)$$

where c is the speed of light, $\tilde{n}_+$ and $\tilde{n}_-$ are the complex refractive indices for the right- and left-circularly polarized components, respectively, and $n_{\pm}$ is the real part of the complex refractive index $\tilde{n}_{\pm}$. Taking into account the contribution to the refractive indices from each hyperfine component,

$$\tilde{n}_{\pm}(\omega) = \sum_{F,F',M} \tilde{n}_{\pm}(\omega, FM, F'M') \quad (10)$$

If $|\tilde{n}_{\pm}(\omega, FM, F'M') - 1|$ is much less than 1, the complex refractive index for the circularly polarized light is

$$\tilde{n}_{\pm}(\omega, FM, F'M') - 1 = CS_{\pm}(FM, F'M')W(\xi_{FM,F'M'}) \tag{11}$$

where $S_{\pm}(FM, F'M')$ is the line strength given in Eq. (4), $W(\xi_{FM,F'M'})$ is the plasma dispersion function given by

$$W(\xi_{FM,F'M'}) = \frac{1}{\sqrt{\pi}} \int_{-\infty}^{\infty} \frac{e^{-x^2}}{x - \xi_{FM,F'M'}}\, dx \tag{12}$$

$$\xi_{FM,F'M'} = \frac{\sqrt{1n2}}{\pi \Delta\nu_D} \left(\omega - \omega_{FM,F'M'} + i\frac{\pi}{\tau}\right) \tag{13}$$

where the transition frequency between the levels FM and $F'M'\omega_{FM,F'M'}$ is calculated from the eigenvalues of the Hamiltonian, and

$$C = \frac{2\pi N(F)}{h(2J+1)(2I+1)\Delta\nu_D} \tag{14}$$

where $\Delta\nu_D$ is the Doppler width, and $N(F)$, the population density of the ground states hyperfine level F (assuming the optical pumping is negligible), is given by

$$N(F) \approx \frac{Ne^{-E(F)/KT}}{\sum_F (2F+1)e^{-E(F)/KT}} \tag{15}$$

where $E(F)$ denotes the ground state hyperfine energy level F, k is Boltzmann's constant, T is the cell temperature in Kelvins, and N is the total rubidium ground-state atomic number density.

The absorption coefficients of the atomic vapor are associated with the imaginary part of the complex refractive index,

$$k_{\pm}(\omega) = \frac{2\omega}{c} Im[\tilde{n}_{\pm}(\omega)] \tag{16}$$

Therefore, the total attenuation of the linearly polarized incident light intensity due to the absorbing medium is

$$a(\omega) = 0.5\left(e^{-k_+(\omega)L} + e^{-k_-(\omega)L}\right) \tag{17}$$

With the crossed polarizers at the ends of the cell, the transmission of the FADOF can be derived. As shown in Fig. 6, the input polarized radiation $\mathbf{E}_{in}$ can be decomposed into left-circular polarization, $\mathbf{E}_+$, and right-circular polarization, $\mathbf{E}_-$. At the input of the cell, we have

$$\begin{aligned} \mathbf{E}_{in} &= E_0\hat{x} \\ &= \frac{E_0}{2}(\hat{x} + i\hat{y}) + \frac{E_0}{2}(\hat{x} - i\hat{y}) \\ &= \mathbf{E}_+(0) + \mathbf{E}_-(0) \end{aligned} \tag{18}$$

After traveling through a FADOF cell of length L, the fields are

$$\begin{aligned} \mathbf{E}_+(L) &= \mathbf{E}_+(0)\ \exp\left[i\frac{\tilde{n}_+(\omega)\omega}{c}L\right] \\ &= \frac{E_0}{2}(\hat{x} + i\hat{y}) \\ &\quad \times \exp\left[-\frac{k_+(\omega)}{2}L + i\frac{n_+(\omega)\omega}{c}L\right] \end{aligned} \tag{19}$$

$$\begin{aligned} \mathbf{E}_-(L) &= \mathbf{E}_-(0)\ \exp\left[i\frac{\tilde{n}_-(\omega)\omega}{c}L\right] \\ &= \frac{E_0}{2}(\hat{x} - i\hat{y}) \\ &\quad \times \exp\left[-\frac{k_-(\omega)}{2}L + i\frac{n_-(\omega)\omega}{c}L\right] \end{aligned} \tag{20}$$

The output field is

$$\begin{aligned} \tilde{E}_{out} &= \mathbf{E}_+(L)\hat{y} + \mathbf{E}_-(L)\hat{y} \\ &= i\frac{E_0}{2}\ \exp\left[-\frac{k_+(\omega)}{2}L + i\frac{n_+(\omega)\omega}{c}L\right] \\ &\quad - i\frac{E_0}{2}\ \exp\left[-\frac{k_-(\omega)}{2}L + i\frac{n_-(\omega)\omega}{c}L\right] \end{aligned} \tag{21}$$

The FADOF transmission is given by

$$T(\omega) = \frac{\tilde{E}\tilde{E}^*}{E_0^2}$$

$$= \frac{1}{4}\Bigg\{\exp\left[-k_+(\omega)L\right] + \exp\left[-k_-(\omega)L\right]$$

$$- 2\cos\left[\frac{n_+(\omega) - n_-(\omega)}{c}\omega L\right]$$

$$\times \exp\left[-\frac{k_+(\omega) + k_-(\omega)}{2}L\right]\Bigg\}$$

$$= \frac{1}{4}\Bigg\{\exp\left[-k_+(\omega)L\right] + \exp\left[-k_-(\omega)L\right]$$

$$-2\cos\left[2\phi(\omega)\right]\exp\left[-\frac{k_+(\omega) + k_-(\omega)}{2}L\right]\Bigg\} \quad (22)$$

where $\phi(\omega)$ is defined in Eq. (9).

In order to compare the FADOF with other types of filters, we define the total equivalent noise bandwidth (ENBW) for the FADOF as

$$ENBW = \frac{1}{T_{max}}\int_{-\infty}^{\infty} T(\omega)d\omega \quad (23)$$

where $T(\omega)$ represents the filter transmission spectrum and $T_{\max}$ represents the maximum transmission for the filter. The equivalent noise bandwidth corresponds to the bandwidth of a rectangular notch filter with transmission $T_{\max}$ that transmits the same amount of noise as our filter. Using the equivalent noise bandwidth, we can easily compare different filter designs and even different filter technologies.

Figure 7 shows the typical calculated spectrum of Rb 780-nm transmission at a temperature of 100 deg C and a magnetic field of 90 G. The calculations include the contribution from both isotopes. The Rb FADOF shown has an equivalent noise bandwidth of 4.7 GHz, a transmission of 93 percent, and a signal bandwidth of 1.3 GHz.

III. Filter Transmission Spectra Measurements Compared With Theory

The FADOF was characterized using a tunable, narrow-linewidth laser diode source. The tuning of a laser diode is accomplished by varying the injection current or the diode temperature. A single-mode 780-nm laser diode (HL7802E) emitting 10 mW of optical power was used in our experiment. The laser diode current and temperature were controlled by a custom-made diode laser controller. The experimental setup is shown in Fig. 8.

A 12.5-cm-long solenoid coil generated the required magnetic field. The magnetic field was controlled by varying the current through the solenoid. A flexible heater strip was used to heat the Rb vapor cell. Two Glan–Thompson polarizers with extinction ratios of 10^{-5} served as the polarizer–analyzer pair. The Rb vapor cell (2.5-cm long) consisted of a small amount of Rb metal in an evacuated cell. Two PIN detectors, located as shown in Fig. 8, were used to simultaneously measure the transmission spectrum of the Rb cell and of the FADOF.

A small triangle-waveform current ramp was superimposed on the laser diode's direct current to sweep the laser emission wavelength across the FADOF transmission spectrum. Knowledge of the Rb hyperfine absorption spectral features allowed the absolute wavelength calibration from the frequency (energy) differences between the absorption peaks of a Rb cell. A typical measurement of the Rb absorption spectrum is shown in Fig. 9.

The FADOF transmission spectrum was calibrated against the measured absorption of the Rb cell. Figure 10 gives the results of such a comparison.

The absolute FADOF transmission was measured by tuning the diode laser frequency to the center frequency of the transmission peak and then measuring both the power transmitted through, and the power incident upon, the FADOF. The ratio of these power measurements provided the absolute FADOF peak transmission. The experimental results were directly compared to the theoretical calculations after correcting for Fresnel reflection losses.

The Rb 780-nm FADOF transmission spectra are shown in Fig. 11 for different combinations of B-field and temperature. The solid lines in the figures are the measured spectra, and the dashed lines are the theoretical calculations. The spectra show good agreement between theory and experiment for all aspects of the filter, bandwidth,

peak transmission, peak center frequency, and spectral response. The theory also predicts the observed 2-GHz tunability of the center frequencies and bandwidths of the FADOF transmission peaks with applied magnetic fields and cell temperatures.

IV. FADOF Imaging and Solar Noise Rejection Measurements

An important advantage of the FADOF over atomic resonance filters is that the FADOF preserves the spatial direction of the signal while filtering out the background noise, but the atomic resonance filter does not [23]. For free-space laser communications applications, this can be used to advantage in the signal acquisition and tracking system. We measured the spatial resolution of the optical system to evaluate its applicability to a signal acquisition and tracking subsystem. A schematic block diagram of the imaging experiment system is shown in Fig. 12.

The target was illuminated by a 3-mW, 780-nm laser diode. A small fraction of the scattered laser light was then incident on both the reference camera and the filtered camera. This system allowed direct comparison of the resolution of images recorded using the unfiltered and filtered cameras. The advantages of the FADOF were demonstrated by comparing the two images as the background light level was changed. The image resolution experiments were performed with the room lights off and using an imaging evaluation test target (Air Force MT-11). The resolution of both cameras was measured to be 170 μrad. Within the 170-μrad resolution limit of our camera, no image degradation resulting from the insertion of the FADOF was observed. Equipment with greater spatial resolution will be needed to measure the resolution limit of the FADOF.

Figure 13 illustrates both the spatial resolution and the background rejection of the FADOF. The solar background rejection was measured at 56 dB. The figure is a photograph of the New Mexico State University (NMSU) logo illuminated by a 3-mW laser diode and a cigarette lighter. Also included in this photograph are the images from both the filtered and unfiltered camera monitors. The unfiltered camera image (upper right) is clearly saturated by the flame of the lighter, while the filtered camera image (lower right) is unaffected by the flame. In addition, the letters "MEX" that are lost in the unfiltered camera image due to the saturation are clearly visible in the filtered camera image. The images were taken with approximately 2-nW/cm^2 of optical power incident on the charge-coupled device (CCD).

V. The Composite Zeeman/FADOF System

The transmission peaks of the FADOF are at the wings of the absorption bands of the atomic vapor. For typical Rb and cesium (Cs) FADOFs, there are four transmission peaks caused by isotopic and hyperfine splitting. Narrowband laser signals are transmitted in one transmission band, and light leakage through the other bands constitutes a source of background noise and adds to the filter's equivalent noise bandwidth. A composite filter system can isolate a single signal transmission band and eliminate the other transmission bands.

In the composite system, a Zeeman absorption cell is placed in series with a FADOF. The Zeeman absorption cell is tuned to absorb three of the four FADOF transmission bands. Optimal operating conditions for the absorption cell were found by calculating the absorption spectra for different combinations of magnetic field and temperature and matching these to the FADOF transmissions.

For right- and left-circularly polarized input, the absorption cell transmission is given as

$$a_{\pm}(\omega) = \exp\left[-k_{\pm}(\omega)L\right] \tag{24}$$

where "+" denotes the right- and "−" denotes the left-circular polarization, k is the absorption coefficient, and L is the cell length. The total transmission of the composite system is

$$T(\omega) = T_{\mathrm{FADOF}}(\omega)a_{\pm}(\omega) \tag{25}$$

where $T_{\mathrm{FADOF}}(\omega)$ is the transmission spectrum of the FADOF.

The block diagram of the composite system for a Rb 780-nm FADOF is shown in Fig. 14. A quarter-wave plate is used to transform the linearly polarized FADOF output to right- or left-circularly polarized input for the absorption cell.

Figure 15 shows the Rb 780-nm FADOF transmission curve at a magnetic field of 60 G and a temperature of 90 deg C. The four transmission peaks of average bandwidth at approximately 0.7 GHz each are characteristic of

this FADOF under these conditions. Calculations showed that the absorption of a Rb Zeeman cell at 100 deg C in a 1300-G B-field could be tuned to match the FADOF transmission peaks and results in a single-peak transmission spectrum.

Figure 16 shows the agreement between the theoretical and experimental absorption curves for right-circularly polarized light incident on the Rb Zeeman cell. The resulting composite filter transmission is shown in Fig. 17.

The single-band transmission spectrum in Fig. 17 was obtained by tuning the system so that the right-circularly polarized absorption band of the Zeeman absorption cell overlapped three of the four transmission peaks in the FADOF transmission spectrum and left the transmission of a single peak unchanged. By cascading the filters in this way, the ENBW was reduced by a factor of 3.5, from 3.0 to 0.86 GHz.

With the end application of the filter in mind, we compared the bandwidth of the composite filter to that of a Fourier-transform-limited Gaussian pulse. This is shown in Fig. 18, where it is seen that a transformed 5-nsec Gaussian pulse just fits under the envelope of the filter. Pulse position modulation is the preferred modulation format for deep space optical communications; this experiment shows that the composite filter can provide good background rejection for detection of 5-nsec-wide laser pulses at the optical communications receiver.

VI. Summary

The FADOF has been shown to be able to provide high background noise rejection, high throughput, fast response, and a wide field of view while preserving image information. The general theory for the FADOF was presented in this article. It predicts the FADOF performance for arbitrary magnetic fields and temperatures of the atomic vapors with and without hyperfine structure components. The theory was used to predict the transmission spectrum and performance of a 780-nm Rb FADOF, based on the solved quantum mechanics equations for the atomic levels and transition line strengths for the Rb vapor. The experimental results show very good agreement with theoretical predictions.

A composite Zeeman–FADOF filter has been described and shown to be compatible with a Fourier-transform-limited 5-nsec laser pulse. The filter pair exhibits a single ultra-narrow passband in the transmission spectrum and is expected to reduce the noise rejection factor of the FADOF by 3.5.

Acknowledgments

The authors wish to thank J. Lesh and K. Wilson in the JPL Optical Communications Group for many helpful discussions and suggestions. Thanks are also expressed to D. C. Yuan and Q. C. Liu for their assistance.

References

[1] D. J. Dick and T. M. Shay, "Ultra-High Noise Rejection Optical Filter," *Opt. Lett.*, vol. 16, p. 867, June 1991.

[2] B. Yin and T. M. Shay, "Theoretical Model of Faraday Anomalous Dispersion Optical Filter," *Opt. Lett.*, vol. 16, pp. 1617–1619, October 1991.

[3] B. Yin and T. M. Shay, "A Potassium Faraday Anomalous Dispersion Optical Filter," *Optics Communications*, vol. 94, pp. 30–32, November 1992.

[4] B. Yin and T. M. Shay, "Faraday Anomalous Dispersion Optical Filter of Cs 455 nm," *IEEE Photonics Technology Lett.*, vol. 4, pp. 488–490, May 1992, and addendum, vol. 5, issue 4, April 1993.

[5] T. M. Shay and B. Yin, "Faraday Anomalous Dispersion Optical Filter," *Proceedings of the International Conference on Lasers '91*, San Diego, California, pp. 641–648, December 1991.

[6] B. Yin and T. M. Shay, "Faraday Anomalous Dispersion Optical Filter of Potassium," *Proceedings of the SPIE OE'Laser '92*, Los Angeles, California, pp. 641–648, January 1992.

[7] T. M. Shay, B. Yin, and L. S. Alvarez, "Faraday Anomalous Dispersion Optical Filter," *International Conference on Lasers '92*, Houston, Texas, pp. 829–836, December 1992.

[8] B. Yin and T. M. Shay, "Theoretical Model for a Novel Ultrahigh Optical Background Rejection Optical Filter," *XVIII International Quantum Electronics Conference*, Vienna, Austria, June 1992.

[9] T. M. Shay and B. Yin, "Theoretical Model for a Faraday Anomalous Dispersion Optical Filter Operating at Ca 423-nm," *IEEE Laser and Electro-Optics Society Annual Meeting*, Boston, Massachusetts, November 1990.

[10] A. M. Title and W. J. Rosenberg, "Improvements in Birefringent Filters," *Appl. Optic.*, vol. 18, pp. 3443–3456, October 1979.

[11] T. M. Shay and Y. C. Chung, "An Ultra-High Resolution, Wide Field-of-View Optical Filter for Doubled Nd:YAG," *Optics Lett.*, vol. 13, p. 443, June 1988.

[12] T. M. Shay and D. Garcia, "Theoretical Model for a Background Noise Limited Rb Laser-Excited Optical Filter for Doubled Nd Lasers," *IEEE J. Quantum Electro.*, vol. 26, p. 1135, June 1990.

[13] M. Minden and H. Bruesselbach, "Detection of 532-nm Frequency-Doubled Nd:YAG Radiation in an Active Rubidium Atomic Resonance Filter," *Optics Lett.*, vol. 15, no. 7, p. 384, April 1990.

[14] J. A. Gelbwachs, "Atomic Resonance Filters," *IEEE J. Quant. Electr.*, vol. 24, p. 1266, July 1988.

[15] A. F. Molisch, B. P. Oehry, W. Schupita, and G. Magerl, "Quantum Efficiency and Signal Bandwidth of Thallium Atomic Line Filters," *Opt. Comm.*, vol. 90, pp. 245–250, June 1992.

[16] D. M. Camm and F. L. Curzon, "The Resonant Faraday Effect," *Can. J. Phys.*, vol. 50, p. 2866, November 1972.

[17] G. J. Roberts, P. E. G. Baird, M. W. S. M. Brimicombe, P. G. H. Sandars, D. R. Selby, and D. N. Stacey, "The Faraday Effect and Magnetic Circular Dichroism in Atomic Bismuth," *J. Phys. B: Atom. Molec. Phys.*, vol. 13, p. 1389, April 1980.

[18] P. Yeh, "Dispersive Magneto-Optic Filters," *Applied Optics*, vol. 21, p. 2069, June 1982.

[19] X. Chen, V. L. Telegdi, and A. Wis, "Magneto-Optical Rotation Near the Cesium D2 Line (Macaluso–Corbino Effect) in Intermediate Fields," *J. Phys. B: At.. Mol. Phys.*, vol. 20, p. 5653, November 1987.

[20] R. D. Cowan, *Theory of Atomic Structure and Spectra*, Berkeley, California: University of California Press, p. 497, 1981.

[21] I. I. Sobelman, *Atomic Spectra and Radiative Transition*, New York: Springer–Verlag, p. 194, 1979.

[22] B. W. Shore, *The Theory of Coherent Atomic Excitation*, vol. 2, New York: John Wiley and Sons, p. 1426, 1990.

[23] L. S. Alvarez and T. M. Shay, "High Resolution Imaging Through an Ultra-High Optical Background Rejection Optical Filter," *OSA 1992 Annual Meeting*, Albuquerque, New Mexico, September 1992.

Table 1. The performance of some narrow bandwidth optical filters.

Parameter	Interference	Quartz Lyot	Atomic resonance	FADOF
Throughput	0.5	0.2	0.1–0.5	>0.8
Noise rejection factor, dB	20–30	35	40–60	50–60
Field of view, deg	±2.5–30	±30	±90[a]	±90[b]
Bandwidth, nm	2–20	0.33	0.001–0.01	0.001–0.005
Response time, nsec	0.00004–0.0004	0.005	10–10,000	0.2–1
Imaging	Yes	Yes	No	Yes

[a] The field of view of the atomic resonance filter is limited to ±30 deg by practical considerations.

[b] The field of view is fundamentally ±90 deg. However, the field of view is limited to about ±20 deg by practical considerations.

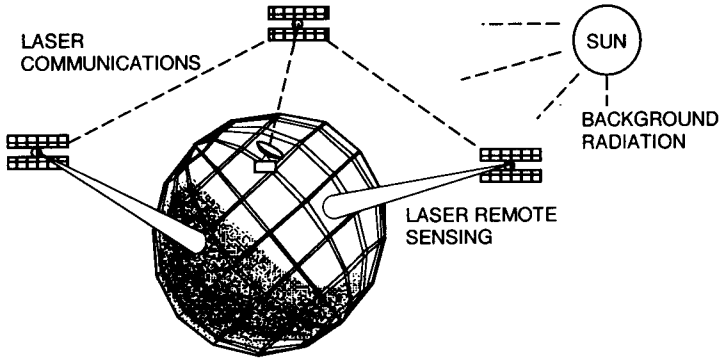

Fig. 1. The broadband, strong solar radiation is the major optical background noise for free-space laser communications and remote sensing.

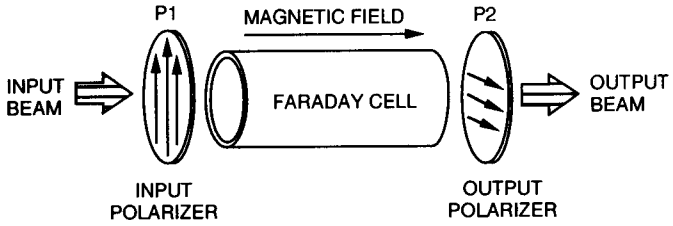

Fig. 2. The Faraday anomalous dispersion optical filter. P1 and P2 are two crossed polarizers.

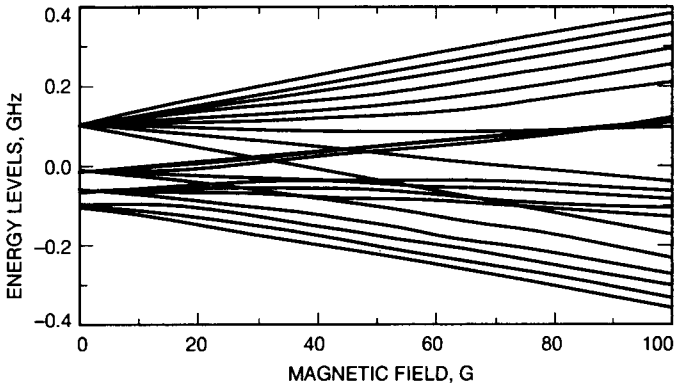

Fig. 4. The calculated $^{85}Rb\ 5^2P_{3/2}$ energy levels versus the magnetic field.

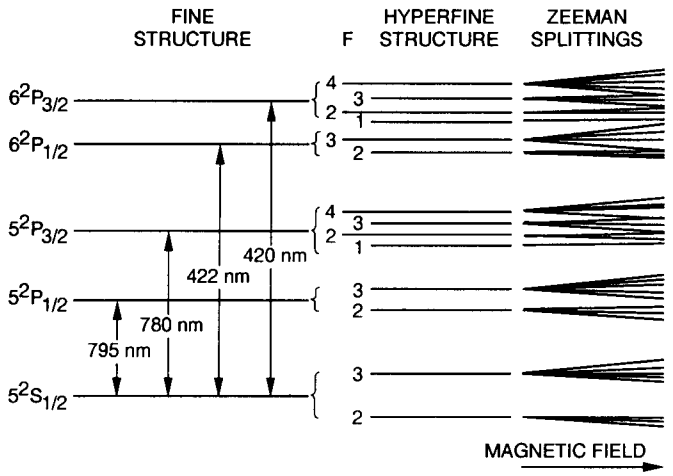

Fig. 3. The simplified energy level diagram for the rubidium near-infrared and blue transitions.

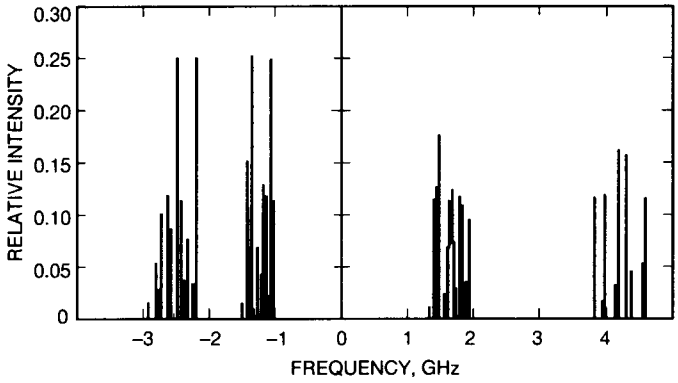

Fig. 5. The ^{85}Rb + ^{87}Rb 780-nm relative hyperfine transition intensities at a magnetic field of 100 G.

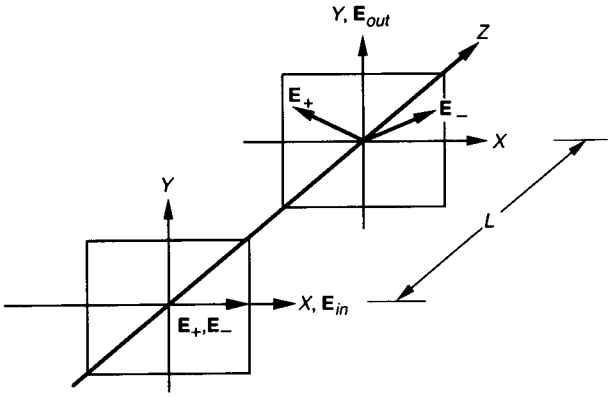

Fig. 6. The rotating fields in the FADOF, where *x* and *y* are the directions of the input and output polarizers and the directions of the input and output polarized radiation, E_{in} and E_{out}, respectively, and *z* is the direction of the magnetic field.

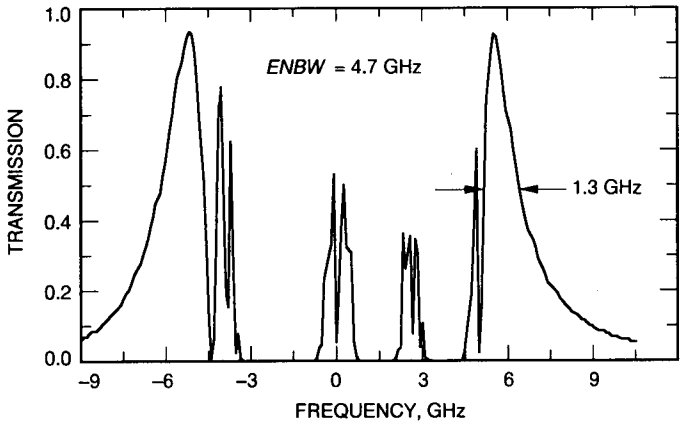

Fig. 7. The calculated Rb 780-nm FADOF transmission at B = 90 G and T = 100 deg C. The maximum transmission is 0.93.

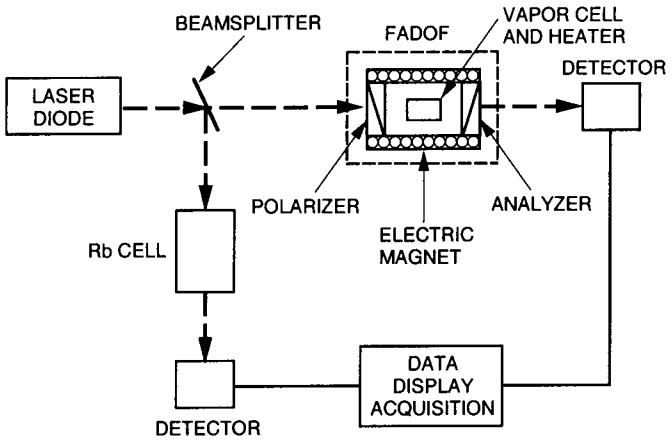

Fig. 8. Experimental setup for the FADOF measurements.

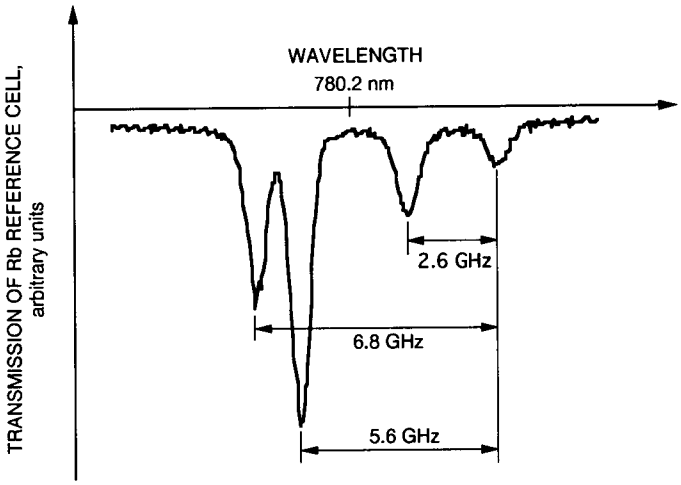

Fig. 9. The transmission spectrum of the absorption cell at a temperature of 300 K .

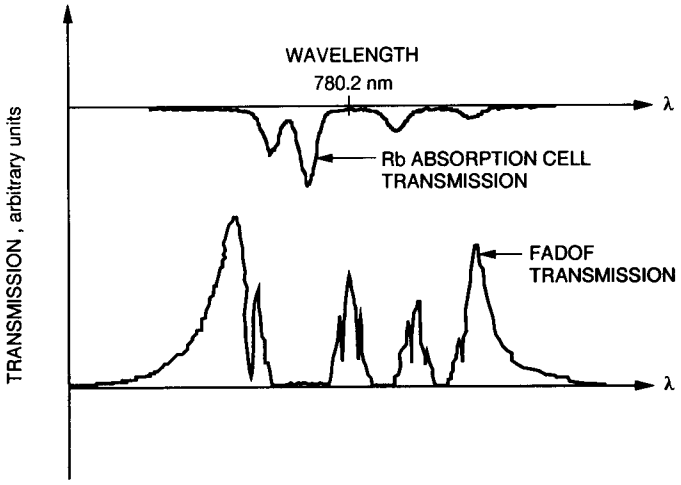

Fig. 10. Experimental measurements of the transmission spectrum of the FADOF. The top curve is measured Rb absorption cell transmission that is used as a frequency reference. The bottom curve is the measured transmission spectrum of the FADOF.

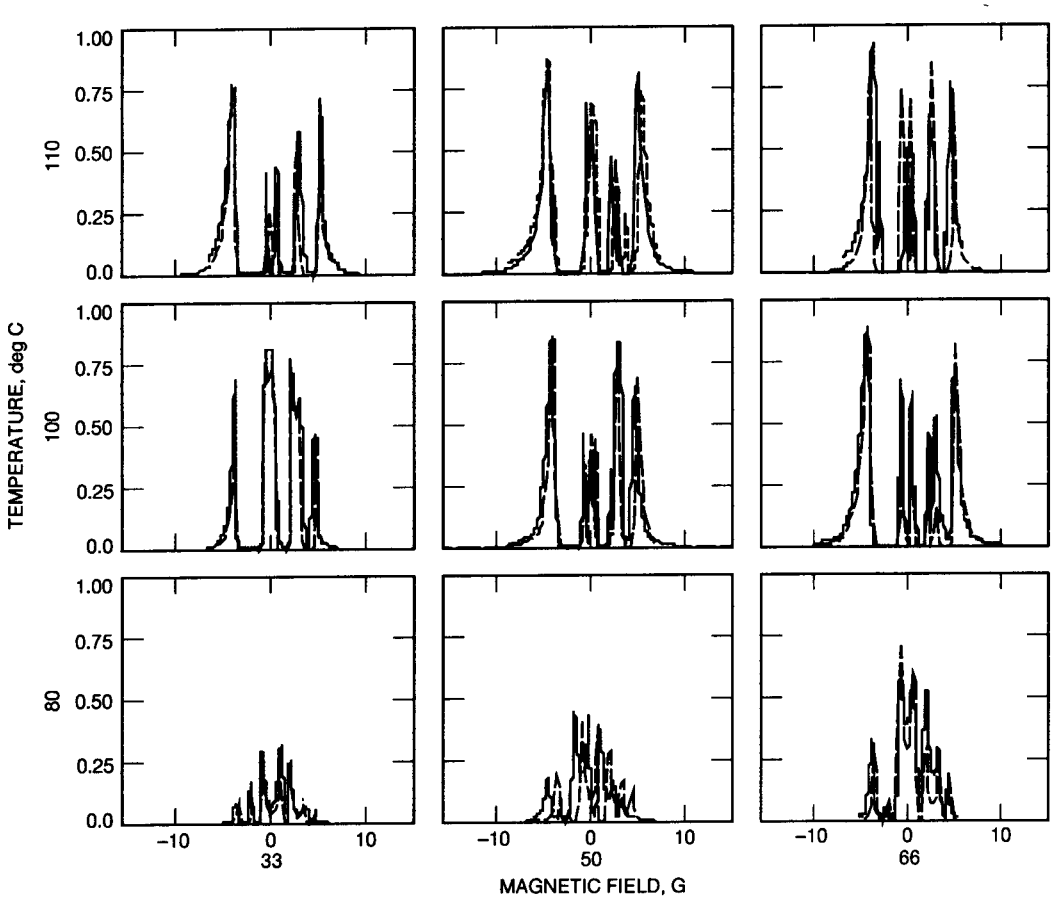

Fig. 11. The transmission curves of the Rb 780-nm FADOF, with the solid lines representing measured transmission and the dashed lines the calculated transmission.

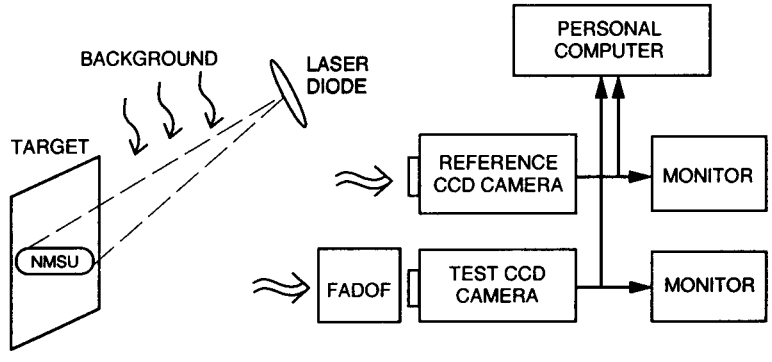

Fig. 12. The FADOF imaging experiment.

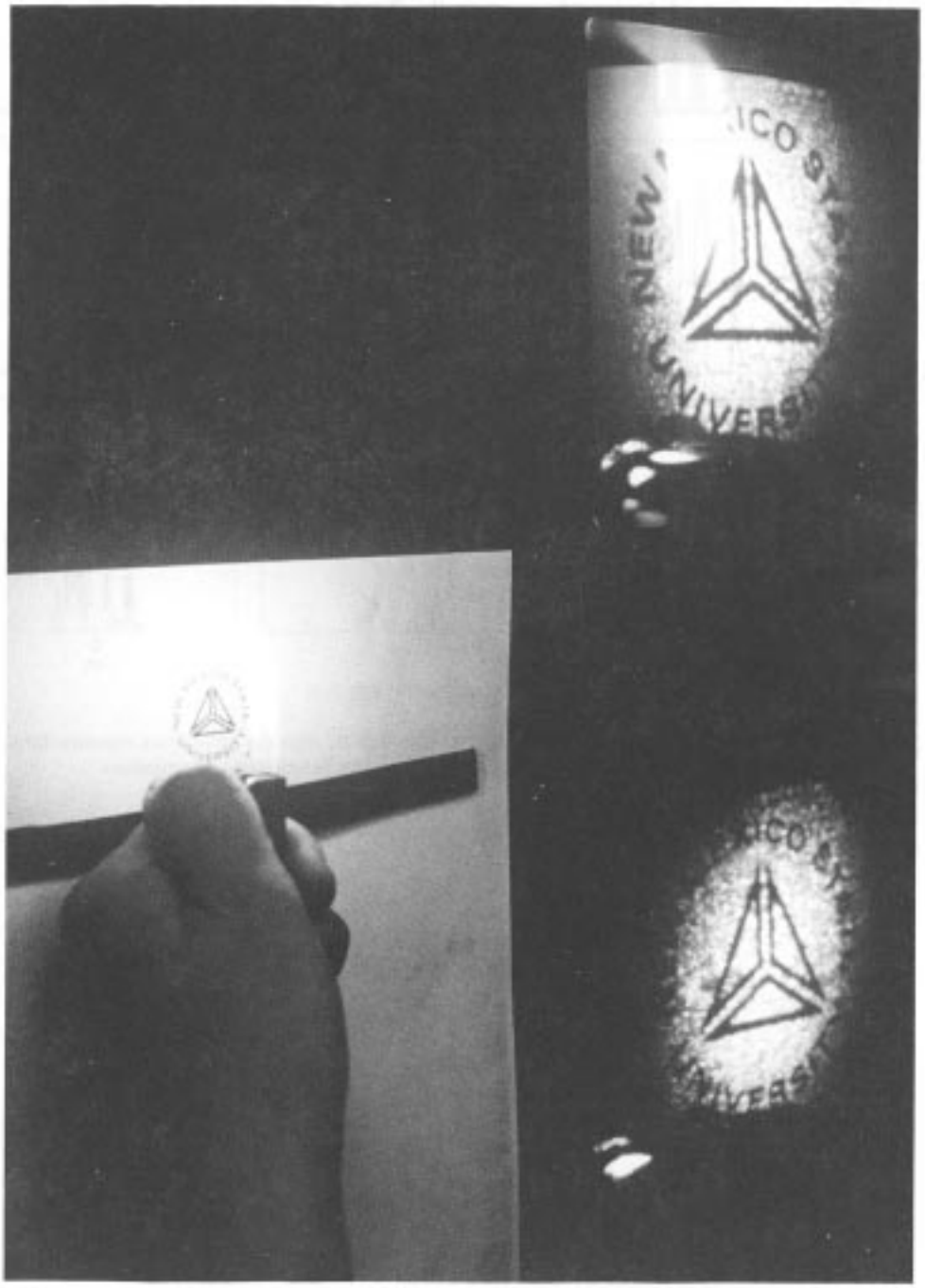

Fig. 13. Images from both filtered and unfiltered camera monitors.

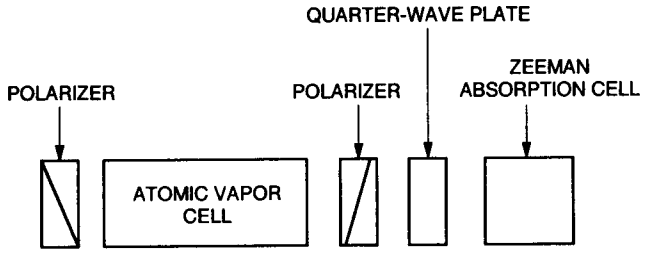

Fig. 14. The composite FADOF/Zeeman system.

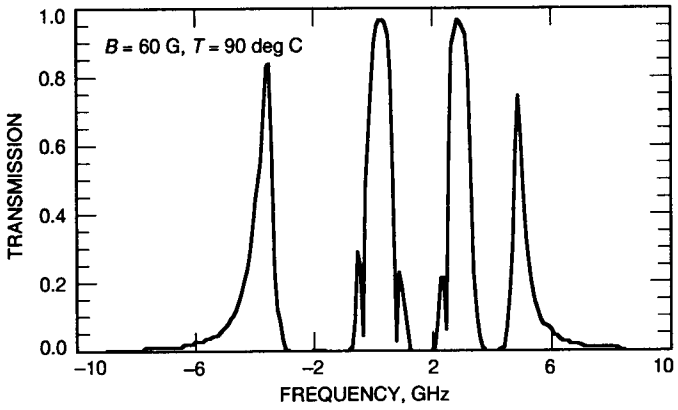

Fig. 15. A Rb 780-nm FADOF transmission with an ENBW of 3.0 GHz.

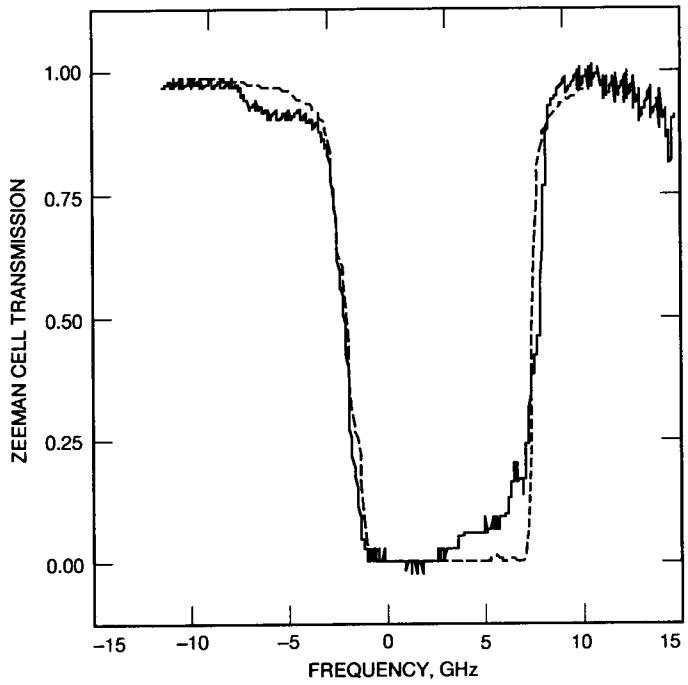

Fig. 16. The transmission spectrum of a Zeeman absorption cell for right-circularly polarized light. The dashed line represents the theoretical curve and the solid line the experimental measurement. The Zeeman cell was operated at a temperature of 100 deg C and a magnetic field of 1300 G.

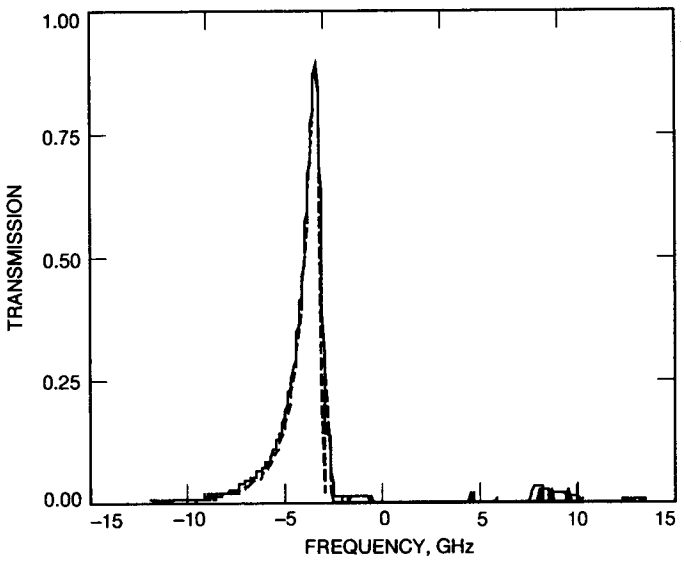

Fig. 17. The transmission spectrum of the Zeeman–FADOF composite filter. The dashed line represents the theoretical curve and the solid line the experimental measurement. The FADOF was operated at a temperature of 100 deg C.

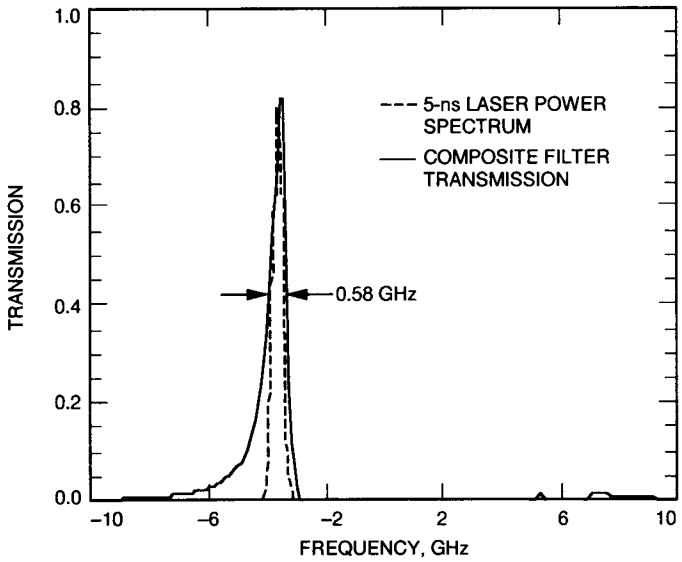

Fig. 18. Total transmission of the Rb composite filter. The ENBW is 0.86 GHz.